Fan-beam filtered-backprojection reconstruction without backprojection weight

Article *in* Physics in Medicine and Biology · July 2007

DOI: 10.1088/0031-9155/52/11/019 · Source: PubMed

4 authors, including:

Frederic Noo
University of Utah
204 PUBLICATIONS **4,211** CITATIONS
SEE PROFILE

Joachim Hornegger
Friedrich-Alexander-University of Erlangen-Nürnberg
688 PUBLICATIONS **14,229** CITATIONS
SEE PROFILE

IOP Publishing Physics in Medicine and Biology

Phys. Med. Biol. **52** (2007) 3227–3240 doi:10.1088/0031-9155/52/11/019

Fan-beam filtered-backprojection reconstruction without backprojection weight

Frank Dennerlein[1], **Frédéric Noo**[1], **Joachim Hornegger**[2] **and Günter Lauritsch**[3]

[1] UCAIR, Department of Radiology, University of Utah, Salt Lake City, UT, USA
[2] Institute of Pattern Recognition, University of Erlangen-Nuremberg, Erlangen, Germany
[3] Siemens AG, Medical Solutions, Forchheim, Germany

E-mail: fdenner@ucair.med.utah.edu

Received 8 January 2007, in final form 27 March 2007
Published 15 May 2007
Online at stacks.iop.org/PMB/52/3227

Abstract

In this paper, we address the problem of two-dimensional image reconstruction from fan-beam data acquired along a full 2π scan. Conventional approaches that follow the filtered-backprojection (FBP) structure require a weighted backprojection with the weight depending on the point to be reconstructed and also on the source position; this weight appears only in the case of divergent beam geometries. Compared to reconstruction from parallel-beam data, the backprojection weight implies an increase in computational effort and is also thought to have some negative impacts on noise properties of the reconstructed images. We demonstrate here that direct FBP reconstruction from full-scan fan-beam data is possible with no backprojection weight. Using computer-simulated, realistic fan-beam data, we compared our novel FBP formula with no backprojection weight to the use of an FBP formula based on equal weighting of all data. Comparisons in terms of signal-to-noise ratio, spatial resolution and computational efficiency are presented. These studies show that the formula we suggest yields images with a reduced noise level, at almost identical spatial resolution. This effect increases quickly with the distance from the center of the field of view, from 0% at the center to 20% less noise at 20 cm, and to 40% less noise at 25 cm. Furthermore, the suggested method is computationally less demanding and reduces computation time with a gain that was found to vary between 12% and 43% on the computers used for evaluation.

1. Introduction

Filtered backprojection (FBP) is a common way to achieve image reconstruction in x-ray computed tomography (CT). For data collected in fan-beam geometry, the FBP may be applied directly, in the measurement geometry (Kak and Slaney 1988, Noo *et al* 2002, Kudo

et al 2002, Pan and Yu 2003, Arai *et al* 2005, Chen *et al* 2006), or indirectly, using first a rebinning of the data from fan-beam geometry to parallel-beam geometry (Kak and Slaney 1988, Besson 1999, Pan 1999). Both approaches, direct and indirect, have their pros and cons, and are currently in use in medical CT scanners. In this paper, we are interested in the direct approach.

One disadvantage of the direct FBP approach is that the backprojection step includes a weighting factor that varies with both the source position and the location where reconstruction is to be performed. This weighting factor is often seen as a source of noise increase, and also makes the direct approach more computationally demanding and more difficult to code in hardware than the indirect approach (Besson 1999, Pan 1999). We have found that flexibility in the FBP formula of Noo *et al* (2002) allows the derivation of a novel direct FBP formula that achieves reconstruction with no backprojection weight, provided the data are collected over 2π. We describe this novel formula assuming a curved detector geometry, which is also called the geometry of equiangular rays in Kak and Slaney's textbook (Kak and Slaney 1988). Conversion of the formula to the geometry of collinear detectors is straightforward and will not be discussed in the paper (see, e.g., Noo *et al* (2002) for details on this conversion).

The paper is organized as follows. In section 2, we give a complete description of the data acquisition geometry, and we recall the expression of two direct FBP formulae, the standard formula given in Kak and Slaney (1988) and the formula in Noo *et al* (2002). In particular, we discuss how these two formulae differ in the way they allow handling of data redundancy, as this feature is the key to the development of our novel formula. More precisely, we show in section 3 that the insertion of a specific data weighting scheme in the formula of Noo *et al* (2002) yields a direct FBP reconstruction formula with no backprojection weight, which is the announced novel formula. Section 4 gives a comparative evaluation of reconstruction performance in terms of resolution, noise and computational effort using computer-simulated fan-beam data of mathematical phantoms. Finally, section 5 briefly summarizes our results and discusses future work.

2. Background

We use the expression $f(\underline{x})$ with $\underline{x} = (x, y)^T$ to describe the spatial distribution of the x-ray linear attenuation coefficient within the imaged object. The reconstruction of this distribution is to be achieved from fan-beam projections that are measured on a curved detector, while the x-ray source and detector rotates as a single assembly around the object. The source is at distance R from the rotation axis and we assume that data acquisition occurs over a complete 2π rotation. The notation $\underline{a}(\lambda) = (R\cos\lambda, R\sin\lambda)^T$ with $\lambda \in [0, 2\pi)$ is used to describe the circular trajectory followed by the focal spot of the x-ray source during data acquisition. Here and throughout the rest of this paper, a superscript T denotes the transpose operator.

Figure 1 illustrates the data acquisition geometry as we picture it: the detector sits on a circle of radius D centered at $\underline{a}(\lambda)$, the rays connecting the source to the detector elements form a fan, and any ray within the fan is specified by an angle $\gamma \in \left[-\frac{\pi}{2}, \frac{\pi}{2}\right]$ that increases in the clockwise direction. The value $\gamma = 0$ corresponds to the central ray of the fan, that is the ray that passes through the origin $\underline{x} = (0, 0)^T$.

For this acquisition set-up, a centered circular field of view (FOV) is determined and we assume the object is compactly supported within this FOV. The FOV radius is just small enough so that all rays that diverge from the source and intersect the FOV hit the detector. The value of $|\gamma|$ for each of the two rays tangent to the FOV is denoted by γ_m; all rays through the FOV are thus defined with $|\gamma| \leqslant \gamma_m$.

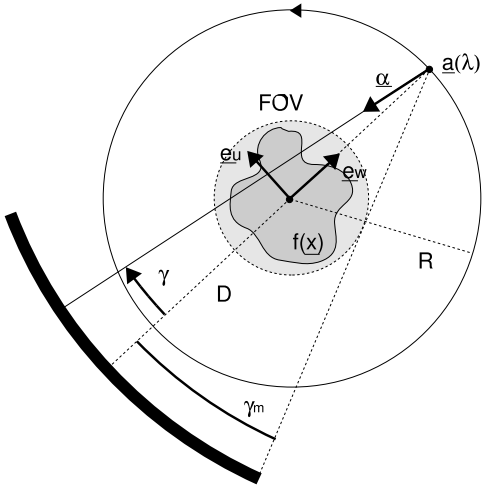

Figure 1. Full-scan fan-beam acquisition geometry with a curved detector. The source describes a circular trajectory of radius R, the detector is at distance D from the source. Each detector element is addressed by a fan-angle γ. The parameters γ and λ specify a ray in the image plane, which originates from $\underline{a}(\lambda)$ and has direction $\underline{\alpha}$.

To mathematically describe the fan-beam data, we introduce a system of two unit orthogonal vectors: $\underline{e}_u(\lambda) = (-\sin\lambda, \cos\lambda)^T$, which is tangent to the source trajectory at $\underline{a}(\lambda)$, and $\underline{e}_w(\lambda) = (\cos\lambda, \sin\lambda)^T$, which gives the direction from the origin $\underline{x} = (0, 0)^T$ toward the source $\underline{a}(\lambda)$. The fan-beam projection at position λ may then be written as

$$g(\lambda, \gamma) = \int_0^{+\infty} f(\underline{a}(\lambda) - t\cos\gamma\,\underline{e}_w(\lambda) + t\sin\gamma\,\underline{e}_u(\lambda))\,\mathrm{d}t. \tag{1}$$

By construction, $g(\lambda, \gamma) = 0$ for $|\gamma| > \gamma_m$, that is no projection is truncated.

The standard direct FBP formula for reconstruction from $g(\lambda, \gamma)$ is

$$f(\underline{x}) = \int_0^{2\pi} \mathrm{d}\lambda \frac{R}{\|\underline{x} - \underline{a}(\lambda)\|^2} \int_{-\gamma_m}^{\gamma_m} \mathrm{d}\gamma\, h_{\mathrm{ramp}}(\sin(\gamma^* - \gamma)) m(\lambda, \gamma)\cos\gamma\, g(\lambda, \gamma). \tag{2}$$

In this equation, $h_{\mathrm{ramp}}(t)$ is the ramp filter, namely the inverse Fourier transform of $|\nu|$, and γ^* is the value of γ for the ray that connects $\underline{a}(\lambda)$ to $\underline{x}$, that is

$$\gamma^* = \tan^{-1}(u^*/D) \qquad \text{with} \qquad u^* = \frac{D\underline{x}\cdot\underline{e}_u(\lambda)}{R - \underline{x}\cdot\underline{e}_w(\lambda)}, \tag{3}$$

where the dot denotes a scalar product.

The function $m(\lambda, \gamma)$ in (2) allows for a proper, explicit handling of redundancies in the fan-beam data. Here, we assume data acquisition over 2π with no projection truncation. Hence, each line integral through the object is measured twice (since any such line has two intersections with the source trajectory) and contributes thus twice to the reconstruction in (2). For formula (2) to be valid, care must be taken to ensure the total contribution of each line to the reconstruction is unity; this is achieved with $m(\lambda, \gamma)$. A common way to ensure unity is to take $m(\lambda, \gamma) = 1/2$, but more sophisticated weights are obviously possible (Crawford and King 1990, Taguchi 2003).

Noo *et al* (2002) suggested another direct FBP formula for reconstruction from $g(\lambda, \gamma)$:

$$f(\underline{x}) = \frac{1}{2\pi}\int_0^{2\pi} \mathrm{d}\lambda \frac{w(\lambda, \underline{x})}{\|\underline{x} - \underline{a}(\lambda)\|} \int_{-\gamma_m}^{\gamma_m} \mathrm{d}\gamma\, h_H(\sin(\gamma^* - \gamma))\hat{g}(\lambda, \gamma). \tag{4}$$

In this equation, $h_H(t)$ is the Hilbert-transform filter, namely the inverse Fourier transform of $-\mathrm{i}\,\mathrm{sgn}(\nu)$, and

$$\hat{g}(\lambda, \gamma) = \left(\frac{\partial}{\partial \lambda} + \frac{\partial}{\partial \gamma} \right) g(\lambda, \gamma). \tag{5}$$

It can be shown (Noo *et al* 2002) that $\hat{g}(\lambda, \gamma)$ is the result of differentiating the fan-beam data with respect to λ while fixing the ray direction $\underline{\alpha}$ (see figure 1).

Function $w(\lambda, \underline{x})$ in (4) plays the same role as function $m(\lambda, \gamma)$ in (2). In contrast with (2) though, the redundancy weighting in (4) applies after the convolution and can thus be carried out in the image domain as part of the backprojection step. This feature allows a definition of the redundancy weight individually for every point $\underline{x}$, yielding increased flexibility in the way data redundancies can be handled. In particular, points that are on the same backprojection ray can be assigned distinct weights without affecting the FBP structure of the reconstruction, which is not possible with the standard FBP formula.

As in the standard case, $w(\lambda, \underline{x})$ must satisfy a normalization condition for (4) to be valid: the total contribution to the final reconstruction of each line passing through $\underline{x}$ must be unity. A common choice for the full-scan is $w(\lambda, \underline{x}) = 1/2$ and we refer to this choice as the uniform weighting approach. However, other choices are possible, as we will discuss in the next section.

3. Direct FBP formula with no backprojection weight

Consider the redundancy weighting function

$$w(\lambda, \underline{x}) = \frac{\|\underline{x} - \underline{a}(\lambda)\|}{2R \cos \gamma^*} \tag{6}$$

as a candidate for reconstruction using Noo's FBP formula (4). The idea is to let the contribution of a given ray to the reconstruction of $f(\underline{x})$ depend on the Euclidean distance between $\underline{x}$ and the source position during the backprojection. As will become clearer below, among all measured rays through $\underline{x}$, the suggested weight gives preference to the fan-beam rays emerging from the source positions that are most away from $\underline{x}$. This preference is accentuated with the distance from $\underline{x}$ to the origin. For reconstruction at $\underline{x} = (0, 0)^T$, however, all rays through $\underline{x}$ are treated equally.

To show that (6) defines a valid weighting function, we need to demonstrate that it normalizes to one the contribution from any line through any point $\underline{x}$ within the FOV. Consider the reconstruction of f at such a point. Then, for any arbitrary source position $\underline{a}(\lambda)$, there exists a complementary source parameter λ_c, such that $\underline{x}$, $\underline{a}(\lambda)$ and $\underline{a}(\lambda_c)$ are collinear and define a line L (see figure 2). The integral along L is acquired twice, at source parameters λ and λ_c, respectively. Using equation (6) to define the weight each measurement on L receives, and using the relation $\gamma_c^* = -\gamma^*$ (see figure 2), we find

$$\begin{aligned} \frac{\|\underline{x} - \underline{a}(\lambda)\|}{2R \cos \gamma^*} + \frac{\|\underline{x} - \underline{a}(\lambda_c)\|}{2R \cos \gamma_c^*} &= \frac{\|\underline{x} - \underline{a}(\lambda)\| + \|\underline{x} - \underline{a}(\lambda_c)\|}{2R \cos \gamma^*} \\ &= \frac{\|\underline{a}(\lambda_c) - \underline{a}(\lambda)\|}{2R \cos \gamma^*} = 1. \end{aligned} \tag{7}$$

The result in (7) proves that (6) defines a valid weighting scheme.

Since the function w we suggest in (6) is proportional to $\|\underline{a}(\lambda) - \underline{x}\|$, it cancels out the backprojection weight $1/\|\underline{a}(\lambda) - \underline{x}\|$ in Noo's FBP formula (4). This means that the computationally costly step of applying the backprojection weight in a direct FBP reconstruction can be avoided. In compensation, the convolved fan-beam data just need to

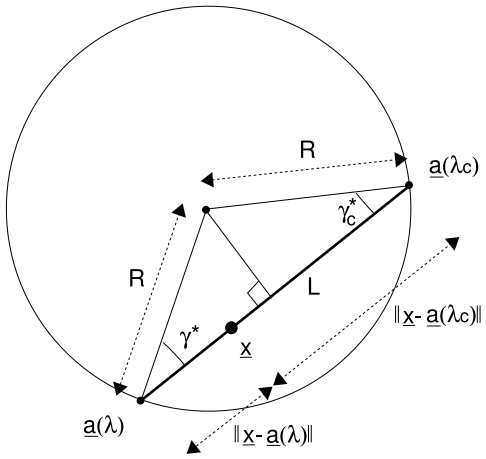

Figure 2. Geometric illustrations of the redundantly measured line L. The line integral corresponding to L is obtained at source parameters λ and λ_c. The absolute value of the fan angle to the line L is identical in both views, λ and λ_c.

be multiplied by $1/(2R\cos\gamma)$ prior to backprojection. Substituting the suggested weighting function (6) into (4) yields the novel direct FBP formula we announced:

$$f(\underline{x}) = \frac{1}{4\pi R}\int_0^{2\pi} g_F(\lambda, \gamma^*)\,\mathrm{d}\lambda \tag{8}$$

where

$$g_F(\lambda, \gamma) = \frac{1}{\cos\gamma}\int_{-\gamma_m}^{\gamma_m} h_H(\sin(\gamma-\omega))\hat{g}(\lambda, \omega)\,\mathrm{d}\omega, \tag{9}$$

with $\hat{g}$ given by equation (5). This formula has no backprojection weight.

4. Evaluation

This section presents an evaluation of the suggested direct FBP formula with no backprojection weight. We refer to this formula as the efficient formula and compare its performance to the application of equation (4) with uniform weighting (namely, $w(\lambda, \underline{x}) = 1/2$), which we refer to as the uniform-weighting formula. The evaluation is performed in terms of spatial resolution, signal-to-noise ratio (SNR) and computational efficiency.

Many geometric factors can affect image quality in fan-beam tomography. These factors include the focal spot size, the anode angle, the size of detector elements, the type of x-ray emission (pulse or continuous) and the source-to-origin distance. For our evaluation, we selected data acquisition parameters that are representative of current medical CT scanners; these parameters are summarized in table 1.

The two formulae we compare were implemented using the same discretization rules. In particular, the computation of $\hat{g}(\lambda, \alpha)$ in equation (5) was performed using the numerical scheme of equation (46) in Noo *et al* (2003). And the Hilbert transform was applied with no apodization, using equation (53) in Noo *et al* (2003). For details on the implementation of the backprojection step, see section 4.3.

Table 1. Fan-beam parameters used for the algorithm evaluation.

X-ray source	
Dimensions (width× height)	1.2 mm ×0.9 mm
Anode angle	7.0°
X-ray emission	continuous
Detector	
No. of pixels	672
Pixel dimensions	1.4083 mm ×1.4083 mm
Detector offset	0.352 075 mm
Source-to-detector distance	$D = 104$ cm
Trajectory	
Radius of the circle scan	$R = 57$ cm
No. of projections	1160

4.1. Comparison of spatial resolution

Predicting differences in spatial resolution performance between the efficient and the uniform-weighting formulae is not straightforward. By omitting the distance-dependent backprojection weight, the efficient formula gives more weight to fan-beam rays for which the source is further away from the point of interest $\underline{x}$. Using the rule of magnification, we could therefore predict a decrease in spatial resolution compared to the uniform-weighting formula, especially in regions far away from the origin of the image coordinate system. However, the efficient formula also favors fan-beam data for which the discretization in λ appears under a smaller angle. Hence, the low-pass effects of continuous x-ray exposure could be less prominent for the efficient formula, and could overall make the efficient formula better in terms of resolution. Altogether, we see thus that argumentation can be given in favor of each reconstruction formula. To clarify the issue, we decided to perform a thorough evaluation of the two formulae in terms of spatial resolution by determining the point spread function (PSF) corresponding to each reconstruction formula at various locations within the FOV.

To obtain the PSF at a specific location $\underline{x}$, a cylindrical object with a tiny circular base was placed at $\underline{x}$. Then, we simulated fan-beam data of this object and achieved from this data reconstruction on a fine Cartesian grid centered at $\underline{x}$. The cylindrical object is intended to be an approximation of the 2D delta function (Dirac impulse). For its radius, we selected 0.15 mm, which is almost ten times smaller than the width of each detector pixel, and for its attenuation coefficient we selected 12.2 mm^{-1}, so that a ray passing through its center suffers an attenuation equivalent to the attenuation caused by a homogeneous water cylinder of 200 mm diameter. Because of discretization effects, the reconstruction of our cylindrical object looks like a blurred spot rather than a disk with a perfectly delineated boundary and this spot represents our estimate of the PSF at $\underline{x}$.

Let us denote by PSF data the fan-beam data of the tiny cylindrical object. To simulate PSF data, all finite-size geometric entities were represented by several points rather than just by their midpoint. In other words, we simulated fan-beam data in an upsampled scenario and subsequently performed binning to obtain PSF data corresponding to the desired sampling pattern and geometric dimensions. In the upsampling scenario, each detector pixel was divided into 14×14 pieces uniformly covering its area, and the focal spot of the x-ray source was divided into a grid of 3×3 subspots. Furthermore, to account for the effect of continuous x-ray emission during data acquisition, five projections were simulated for each

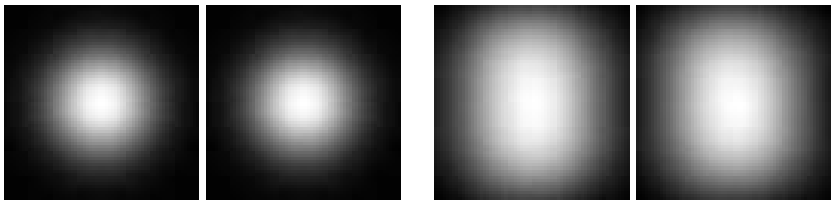

Figure 3. Point spread function (PSF) at position $(0.5\,\text{cm}, 0\,\text{cm})^T$ (left two images) and at position $(24.5\,\text{cm}, 0\,\text{cm})^T$ (right two images). In each case, the PSF corresponding to the uniform-weighting formula is on the left side, while the PSF for the efficient formula is on the right side.

fan-beam projection, using five different positions for the focus–detector assembly, which were uniformly distributed over $2\pi/1160$ around the nominal position for the desired projection. Altogether, 8820 line integrals were thus computed to simulate each PSF data sample, and binning proceeded by first converting these line integrals into attenuation factors.

The PSF estimate at an arbitrary position of interest $\underline{x}$ was obtained on a Cartesian grid of 64×64 square pixels of side 0.04 mm. For a detailed analysis, we extracted profiles of the PSF along half-lines, with each half-line starting at $\underline{x}$ and describing some angle ω with the x-axis. Let p be the distance from $\underline{x}$ along each half-line; typically, the extracted profiles are monotonously decreasing functions of p with maximum value at $p = 0$ i.e., at point $\underline{x}$. Hence, a coordinate p_{half} at which half the maximum value is reached may be defined. This coordinate, p_{half}, characterizes the spatial extent of the PSF as a function of angle ω and we call $2p_{\text{half}}$ the full-width at half maximum (FWHM) of the PSF at ω. If the PSF were a radial function, the FWHM would be independent of ω. However, this is not the case in our evaluations. Hence, we computed the FWHM for 256 profiles corresponding to ω values uniformly sampled over the interval $[0, 2\pi)$. The mean value of the obtained 256 FWHMs as well as their standard deviation were then computed as a characterization of the achievable spatial resolution at $\underline{x}$.

Due to the symmetry of the full-scan reconstruction problem, the spatial resolution is essentially a radial function i.e., a function only of the distance d from the origin. To compare the resolution given by the two formulae over the complete FOV, PSFs were generated and evaluated as explained above at 25 different distances d, starting at $d = 0.5$ cm and incrementing in steps of $\Delta d = 1.0$ cm. For convenience, all PSFs were located on the positive side of the x-axis.

Figure 3 shows the PSFs obtained with the uniform-weighting formula and the efficient formula at two locations, $d = 0.5$ cm and $d = 24.5$ cm, while variations in the PSF shape across the FOV are presented in figure 4, using the FWHM concept. In particular, figure 4 includes a plot of the ratio between the FWHM given by each formula at each sampled ω; both mean and standard deviation of this ratio are displayed.

The results show that both formulae yield a very similar resolution across the FOV. Near the origin, a nearly radial PSF of FWHM smaller than 1.2 mm is obtained. As d increases, the mean of the FWHMs continuously increases to reach a value of approximately 1.9 mm at the edge of the FOV. Furthermore, the standard deviation of the FWHMs over all profile angles gets larger, indicating a decrease in PSF symmetry. We note that this decrease appears slightly worse when using the uniform-weighting formula. The ratio between the FWHMs shows there is less than 2% difference in resolution between the uniform-weighting formula and the efficient formula. This difference is in favor of the efficient formula in region $d < 200$ mm, and in favor of the uniform-weighting formula in region $d > 200$ mm. In length units, the worst difference in FWHM is 0.025 mm.

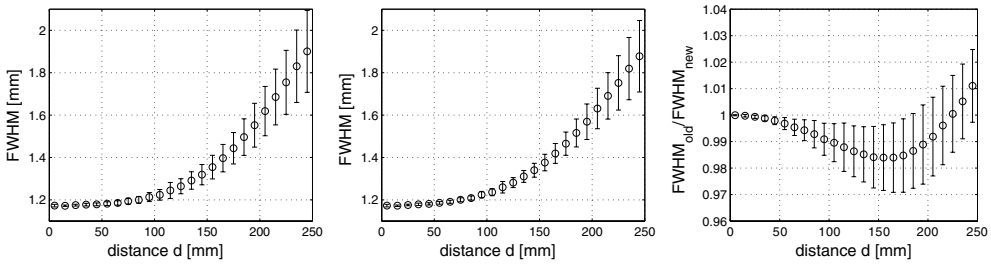

Figure 4. Mean value and standard deviation of FWHMs obtained from 256 radial profiles through the PSF. These quantities are shown as a function of d, the distance from the PSF to the origin. (Left) Using the uniform-weighting approach. (Middle) Using the efficient formula. (Right) Ratio of the FWHMs ('uniform-weighting' over 'efficient').

4.2. Comparison of discretization errors and noise propagation

Discretization errors and noise propagation were investigated using reconstructions from noisy fan-beam data of a slice through the FORBILD thorax phantom. For this investigation, the size of the phantom was enlarged using a bigger ellipse for the body contour; the new ellipse was of size 49 cm by 28 cm, and was centered at $(0\,\text{cm}, 2\,\text{cm})^T$. The reconstructions were performed from 800 distinct noise realizations, each on a Cartesian grid of square pixels of side 0.75 mm. Thus, 800 images were obtained from each reconstruction formula. Variations in the intensities of each pixel across these 800 images give statistics on the uncertainty that can be expected in the reconstruction of the real, sought density function at each pixel location, due to data noise.

Data simulation for each noise realization was performed as in section 4.1, using upsampling and then binning to model all geometric factors. The upsampling parameters were the same as in section 4.1, except for the detector pixels which were represented each by a Cartesian grid of 3×3 subpixels (instead of 14×14), to speed up the simulation. Poisson noise was added to the noise-free fan-beam data after binning to the desired dimensions, assuming an emission of 150 000 photons per ray.

Figure 5 (left) shows the mean of the 800 reconstructions obtained from each formula. These means are displayed using a highly compressed grayscale to exhibit the discretization errors. Compared to the ground-truth, which is also displayed in figure 5, we observe that both formulae perform very well. However, the uniform-weighting formula yields a bit more discretization errors away from the origin (see the regions within the dashed circles).

Figure 5 (right) shows the reconstructions obtained from each formula when using only a single set of noisy data. In each figure, differences in noise level that increase with the distance from the origin can be observed between the two reconstructions. To analyze further these differences, we computed on a pixelwise basis the standard deviation across the 800 reconstructions obtained from each formula. Figure 6 shows the resulting standard deviation images, and figure 7 shows the ratio between these images, again computed pixelwise. These figures show that each formula yields a similar standard deviation near the FOV center, but away from this center the efficient formula performs better. At a distance of 15 cm from the origin, reconstructions from the uniform-weighting formula show a 5% higher noise level compared to the efficient formula and this percentage increases rapidly with the distance from the origin; the percentage is 20% at 20 cm and as high as 40% at 25 cm. Hence, the efficient formula is more robust to noise than the uniform-weighting formula, and the difference in robustness is not negligible off-center.

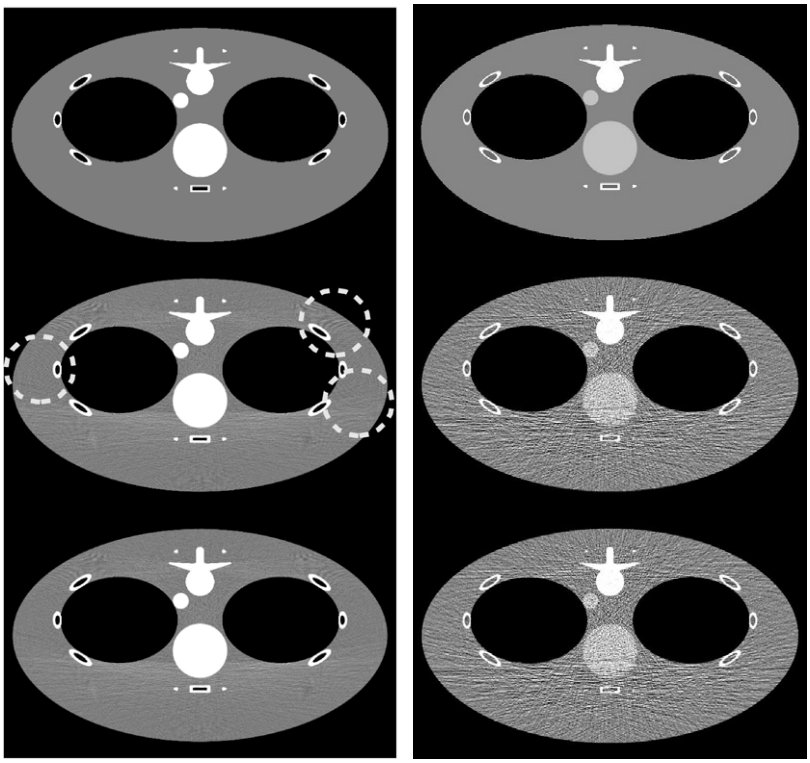

Figure 5. Reconstructions of the slice $z = 0$ cm through the FORBILD thorax phantom with enlarged body contour. (Left) Comparison between the ground truth and the mean over 800 reconstructions obtained from distinct noise realizations; grayscale: $[-20, 20]$ HU. (Right) Comparison between the ground truth and the reconstruction obtained from a single noisy data set; grayscale: $[-110, 100]$ HU. In each case, left and right, the top image is the ground truth, the middle image is the result from the uniform-weighting formula, and the bottom image is the result from the efficient formula. The three dashed circles in the middle image of the left column indicate regions where the reconstruction with the uniform-weighting formula exhibits slight differences in discretization errors.

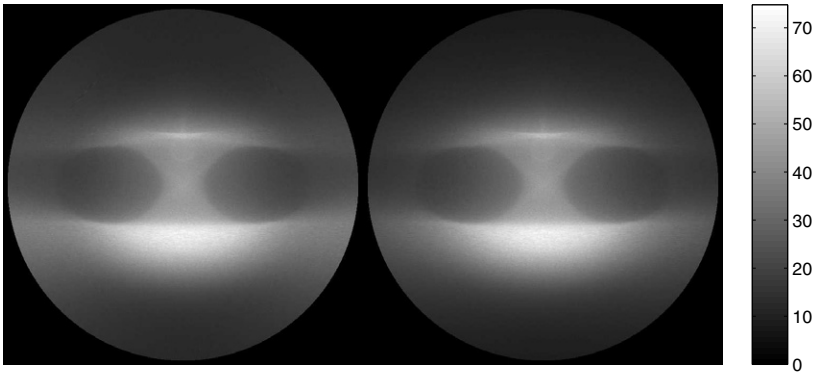

Figure 6. Standard deviation images obtained from reconstructions of the FORBILD thorax phantom with enlarged body contour; 800 distinct Poisson noise realizations were considered with 150 000 photons per ray. (Left) Result for the uniform-weighting formula. (Right) Result for the efficient formula.

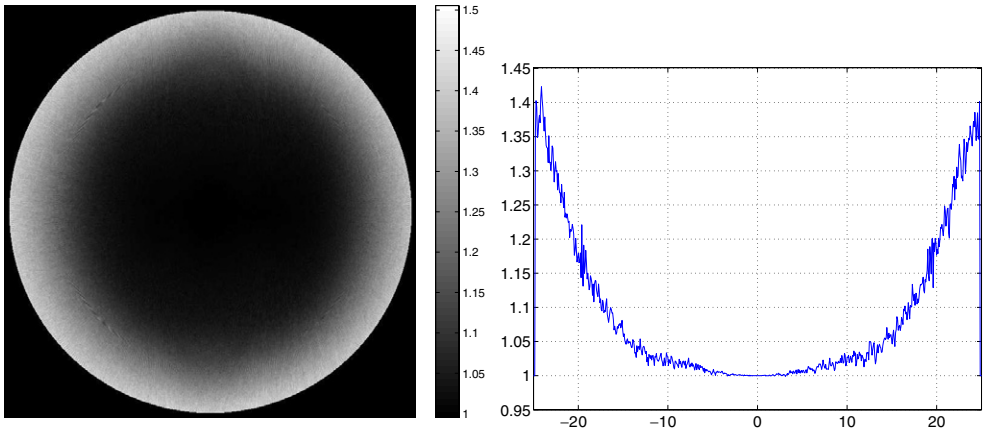

Figure 7. Close inspection of the standard deviation images in figure 6. (Left) Noise behavior comparison using pixelwise computation of the ratio between the standard deviation images ('uniform-weighting' over 'efficient'). (Right) Plot along the central horizontal line of the ratio image shown to the left.

Technically, noise properties should be compared at equal spatial resolution, which is not achieved according to the results in section 4.1. However, these results show that resolution, if not equal, is at least very similar, so much that the gain observed in standard deviation may not be the cause of differences in resolution. In particular, note that if the difference in resolution was thought to be the cause of the difference in standard deviation, then this latter difference should follow the shape of the PSF plot in the right side of figure 4. Nevertheless, we have investigated resolution matching through a modeling of the PSFs as Gaussian functions. As expected, this investigation yielded no measurable difference in standard deviation.

4.3. Computational efficiency

The efficiency of the two reconstruction formulae was evaluated using direct counting of the number of required additions, multiplications and divisions, and also using measurements of execution times on three different systems. We concentrated this evaluation on the backprojection step since this step is typically the most demanding one, and furthermore the significant difference between the two reconstruction formulae lies in the backprojection step.

Clearly, any evaluation of efficiency depends on the amount of sophistication attached to the implementation of the reconstruction formulae. For example, a direct implementation of the uniform-weighting formula based on (4) is bound to be much slower than a direct implementation of the efficient formula because the backprojection weight in (4) requires the computation of a square root for each source position for each pixel. We aimed at a deeper comparison and decided to use the following relation in the implementation of the uniform-weighting formula (Noo *et al* 2003):

$$\|\underline{a}(\lambda) - \underline{x}\| = \frac{R - x\cos\lambda - y\sin\lambda}{\cos\gamma^*}. \tag{10}$$

Using this relation yields a much more efficient implementation of the uniform-weighting formula as the square root is avoided and the $\cos\gamma^*$ factor can be taken care of prior to backprojection by just multiplying the filtered data by $\cos\gamma$.

```
   Input: Filtered data: g_F(λ, γ)
   Output: Reconstruction: f(x)
 1 g_1(λ, γ) = cos γ g_F(λ, γ) ;
 2 g_2(λ, u) = g_1(λ, tan^{-1}(u/D)) ;
 3 foreach Projection λ do
 4     T_1 = Δx sin λ * (D/Δu);
 5     T_2 = Δx cos λ;
 6     foreach Row in the image y do
 7         Initialize NUM, DEN;
 8         foreach Column in the image x do
 9             if (x,y) ∈ ROI then
10                 W = 1/DEN ;
11                 û = NUM * W ;
12                 U_idx = û + U_0 ;
13                 f(x, y)+ = g_2(λ, U_idx) * W ;
14             end
15             NUM = NUM − T_1;
16             DEN = DEN − T_2;
17         end
18     end
19 end
```

```
   Input: Filtered data: g_F(λ, γ)
   Output: Reconstruction: f(x)
0.1 g_1(λ, γ) = g_F(λ, γ)/ cos γ;
0.2 g_2(λ, u) = g_1(λ, tan^{-1}(u/D)) ;
0.3 foreach Projection λ do
0.4     T_1 = Δx sin λ * (D/Δu);
0.5     T_2 = Δx cos λ;
0.6     foreach Row in the image y do
0.7         Initialize NUM, DEN;
0.8         foreach Column in the image x do
0.9             if (x,y) ∈ ROI then
0.10                û = NUM/DEN ;
0.11                U_idx = û + U_0 ;
0.12                f(x, y)+ = g_2(λ, U_idx) ;
0.13            end
0.14            NUM = NUM − T_1;
0.15            DEN = DEN − T_2;
0.16        end
0.17    end
0.18 end
```

Figure 8. Pseudo-code for the backprojection step corresponding to (left) the uniform-weighting formula and (right) the efficient formula. The resampled data $g_2(\lambda, u)$ are defined with a sampling distance Δu and the quantity $\hat{u} = u^*/\Delta u$ gives the detector coordinate where $\underline{x}$ is projected to, measured in multiples of Δu. The quantity *NUM* is the numerator of u^* in (3), divided by Δu; *DEN* stands for the denominator in (3). The increments that *NUM* and *DEN* experience when incrementing x at fixed y are defined by T_1 and T_2. Initialization of *NUM* and *DEN* refers to their calculation from the current value of y and the first sampled value in x. Finally, note that U_0 denotes in pixel units the location where the origin projects to, so that U_{idx} gives the index of the sample closest to $\hat{u}$.

Now, note that a direct implementation of both formulae requires the computation of an inverse tangent to obtain γ^* from u^* in (3). When using (10), this requirement largely dominates the effort for the backprojection weight in the uniform-weighting formula, so that little difference could be observed between the two reconstruction formulae. This issue was circumvented by resampling the filtered data on a fine grid in $u = \tan\gamma$ prior to backprojection. This resampling not only eliminates the need to compute the inverse tangent but also enables us to access data during backprojection using nearest-neighbor interpolation rather than the more costly linear interpolation.

A sketch of our implementation of the two reconstruction formulae is given in figure 8. In addition to avoiding the square root and the inverse tangent, these sketches also show that we aimed at a minimization of the number of operations within the most inner loop, as this number has major impact on computation time. For the uniform-weighting formula, one division (line 10), two multiplications (lines 11 and 13) and four additions (lines 12, 13, 15 and 16) are required[4]. For the efficient formula, one division (line 0.10) and four additions (lines 0.11, 0.12, 0.14, 0.15) are required. Hence, in terms of operations, there is a gain of two multiplications out of seven operations total in favor of the efficient formula.

How the gain observed in the number of operations converts into actual benefits on real systems is not trivial, as it highly depends on the system architecture, on the status of the system at initialization time, on the compiler and on internal optimizations transparent to the software developer. For illustration, a C-implementation of both formulae was tested on three different platforms, called Vanda, Hailfire and Anakin. These platforms all operated

[4] The division plus the two multiplications could be replaced by two divisions, but the outcome was slower on the systems we used.

Table 2. Execution times for the two algorithms ('Unif.' and 'Effic.' denote the uniform-weighting and the efficient formula, respectively) on three different systems as absolute values (in seconds) and as a ratio (uniform-weighting over efficient).

	Filtering			Backprojection			Total		
	Unif.	Effic.	Ratio (%)	Unif.	Effic.	Ratio (%)	Unif.	Effic.	Ratio (%)
Vanda	0.711	0.723	98.3	4.483	3.873	115.7	5.194	4.596	113.0
Hailfire	0.655	0.661	99.1	3.394	2.842	119.4	4.048	3.503	115.5
Anakin	0.707	0.713	99.2	6.447	3.371	191.3	7.154	4.084	175.2

under Linux, and we compiled each code separately on each of them using the C compiler of the GNU library (gcc) while enabling code optimization using the compiler option -O4. After compilation, the code was executed 20 times for reconstruction on a Cartesian grid of 512×512 square pixels of side 1 mm, assuming a centered circular region-of-interest (ROI) of radius 25 cm (the object was a water cylinder of radius 24 cm). The mean CPU time of the 20 executions was recorded on each of the three systems, and is presented in table 2. Not surprisingly, significant differences were observed from one platform to the other, with the global gain in favor of the efficient formula being as high as 43% on Anakin. Note that Vanda has a 32-bit Intel Pentium 4 CPU with 3.40 GHz, 1 MB cache and 2 GB RAM; Hailfire has a 64-bit AMD Opteron CPU with 2.00 GHz, 1 MB cache and 7 GB RAM; and Anakin has a 64-bit Intel Pentium 4 CPU with 3.30 GHz, 2 MB cache and 4 GB RAM.

5. Discussion and conclusion

We developed a novel direct FBP formula that allows full-scan fan-beam reconstruction with no backprojection weight. The development was based on Noo's fan-beam FBP formula (Noo *et al* 2002). In contrast to the standard direct FBP formula with ramp filter (Kak and Slaney 1988), this formula has the data-redundancy weighting operation embedded in the backprojection step. This allows the attribution of different weights to points that lie on a same backprojection ray without affecting the FBP structure of the reconstruction. We showed that this feature authorizes the use of a weighting function that cancels out the backprojection weight in Noo's formula, thus yielding the novel formula.

The performance of our novel formula was evaluated against the use of Noo's formula with uniform weighting of data redundancy. We observed a gain in terms of computation time in a software implementation: depending on the system used this gain varied from 14% to 47% in backprojection effort with no significant difference in filtering time. A gain may also be expected in a hardware implementation, but quantification of this gain was not performed. Besides efficiency gain, we also observed a gain in terms of noise properties: the standard deviation on the reconstructed values was reduced by a factor that rapidly increases from 0% at the center of the FOV to 40% at the edge of the FOV; this improvement may be significant for large patients. On the other hand, spatial resolution and discretization errors appeared very similar across the FOV.

We have not compared our novel formula against the classical fan-beam FBP method described in Kak and Slaney (1988). However, a superior performance may be anticipated, both in computation time and in image quality. The gain in computation time is straightforward since our formula does not require any backprojection weight, while the effort in data filtering is essentially the same. For the gain in image quality, we refer the reader to the paper of Zamyatin *et al* (2006), which shows that the classical formula is less robust to data noise

and discretization errors than the uniform-weighting formula, which we compared the novel formula to. To achieve this superiority in image quality, it may however be needed to compute $\hat{g}(\lambda, \gamma)$ in equation (5) using the approach suggested in Zamyatin *et al* (2006) rather than our discretization scheme.

Recently, several new direct and indirect fan-beam reconstruction formulae have been suggested (Pan 1999, Pan and Yu 2003, Wang *et al* 2005, You *et al* 2007). These formulae were shown each to achieve improvements in image quality over the classical fan-beam FBP formula. It would therefore be of interest to compare their performance to that of our formula, and we may perform such a comparison in the future.

The novel formula was derived exclusively for reconstruction from full-scan fan-beam data. Direct fan-beam FBP reconstruction with no backprojection weight may not be possible when the data are only measured on a short-scan or a super short-scan. However, partial elimination of the backprojection weight may be achieved using the same data weighting strategy as presented here. More specifically, the backprojection weight in Noo's formula (2002) can be eliminated for each ray that corresponds to a line integral that is measured twice, by weighting each such ray with function $w(\lambda, \underline{x})$ of equation (6) during the backprojection. On the other hand, for the rays that correspond to line integrals that are only measured once, only $w(\lambda, \underline{x}) = 1$ can be applied, so that our approach does not allow elimination of the backprojection weight for singly-measured rays.

Acknowledgments

This work was partially supported by a grant of Siemens AG, Medical Solutions and by the US National Institutes of Health (NIH) under grants R21 EB000568 and R01 EB000627. Its contents are solely the responsibility of the authors.

References

Arai I, Kudo H, Noo F, Defrise M and Pack J D 2005 A new class of super-short-scan algorithms for fan-beam reconstruction *Proc. IEEE NSS* pp 2296–300

Besson G 1999 CT image reconstruction from fan-parallel data *Med. Phys.* **26** 415–26

Chen G H, Tokalkanahalli R and Hsieh J 2006 Development and evaluation of an exact fan-beam reconstruction algorithm using an equal weighting scheme via locally compensated filtered backprojection (LCFBP) *Med. Phys.* **33** 475–81

Crawford C F and King K F 1990 Computed tomography scanning with simultaneous patient translation *Med. Phys.* **17** 967–82

Kak A C and Slaney M 1988 *Principles of Computerized Tomographic Imaging* (Piscataway, NJ: IEEE Press)

Katsevich A 2002 Analysis of an exact inversion algorithm for spiral cone-beam CT *Phys. Med. Biol.* **47** 2583–97

Katsevich A, Taguchi K and Zamyatin A A 2006 Formulation of four Katsevich algorithms in native geometry *IEEE Trans. Med. Imaging* **25** 855–68

Kudo H, Noo F, Defrise M and Clackdoyle R 2002 New super-short-scan algorithm for fan-beam and cone-beam reconstruction *Proc. IEEE MIC* pp 902–6

Noo F, Defrise M, Clackdoyle R and Kudo H 2002 Image reconstruction from fan-beam projections on less than a short scan *Phys. Med. Biol.* **47** 2525–46

Noo F, Pack J D and Heuscher D 2003 Exact helical reconstruction using native cone-beam geometries *Phys. Med. Biol.* **48** 3787–818

Pan X 1999 Optimal noise control in and fast reconstruction of fan-beam computed tomography image *Med. Phys.* **26** 689–97

Pan X and Yu L 2003 Image reconstruction with shift-variant filtration and its implication for noise and resolution properties in fan-beam computed tomography *Med. Phys.* **30** 590–600

Taguchi K 2003 Temporal resolution and the evaluation of candidate algorithms for four-dimensional CT *Med. Phys.* **30** 640–50

Wang J, Lu H, Li T and Liang Z 2005 An alternative solution to the nonuniform noise propagation problem in fan-beam FBP image reconstruction *Med. Phys.* **32** 3389–94

You J and Zeng G L 2007 Hilbert transform based FBP algorithm for fan-beam CT full and partial scans *IEEE Trans. Med. Imaging* **32** 3389–94

Zamyatin A A, Taguchi K and Silver M D 2006 Practical hybrid convolution algorithm for helical CT reconstruction *IEEE Trans. Nucl. Sci.* **53** 167–74